Atmospheric Environment 98 (2014) 242–252

Contents lists available at ScienceDirect

Atmospheric Environment

journal homepage: www.elsevier.com/locate/atmosenv

Altitudinal effect to the size distribution of water soluble inorganic ions in PM at Huangshan, China

Li Li [a], Yan Yin [a, b, *], Shaofei Kong [a, b], Bin Wen [a], Kui Chen [a], Liang Yuan [a], Qi Li [a]

[a] Key Laboratory for Aerosol-Cloud-Precipitation of China Meteorological Administration, School of Atmospheric Physics, Nanjing University of Information Science and Technology, Ningliu Road 219, Nanjing, China
[b] Collaborative Innovation Center on Forecast and Evaluation of Meteorological Disasters, Nanjing University of Information Science & Technology, Nanjing 210044, China

HIGHLIGHTS

- Size-fractioned water-soluble inorganic ions in PM on Huangshan, China.
- Mass concentrations of particles and ions decreased with altitude increasing.
- SO_4^{2-}, NH_4^+ and NO_3^- presented different distribution at different altitudes.
- Aerosol acidity was analyzed and compared with other mountainous sites.

ARTICLE INFO

Article history:
Received 15 June 2014
Received in revised form
27 August 2014
Accepted 28 August 2014
Available online 29 August 2014

Keywords:
Water-soluble inorganic ions
Size-fractioned aerosol
Vertical distribution
Huangshan

ABSTRACT

To investigate the vertical variation of water soluble inorganic ions (WSI) in aerosols at a regional background mountainous site, nine size fractions of particles (10.0–9.0, 9.0–5.8, 5.8–4.7, 4.7–3.3, 3.3–2.1, 2.1–1.1, 1.1–0.65, 0.65–0.43 and <0.43 μm) were collected at two different altitudes simultaneously at Huangshan in southeast China, from 14 September to 26 October of 2012. The mass concentrations of $PM_{1.1}$, $PM_{2.1}$ and PM_{10} were 17.07, 21.28 and 39.25 μg/m^3 at the summit (SM, 1840 m), respectively and were 24.79, 29.02 and 42.39 μg/m^3 at a lower height site (LL, 869 m). The average mass concentrations of total WSI for $PM_{1.1}$, $PM_{2.1}$ and PM_{10} were 9.59, 11.73 and 17.16 μg/m^3 at SM, and were 16.88, 19.38 and 27.61 μg/m^3 at LL. The concentrations of particulates and WSI both decreased with altitude increasing from 869 m to 1840 m. SO_4^{2-} and NH_4^+ exhibited peak values 0.43–0.65 μm at SM, whereas maintained peak values 0.65–1.1 μm at LL. NO_3^- were mostly concentrated in fine mode for SM but in coarse mode for LL. Further analyses showed that at LL, the heterogeneous reaction on coarse particles containing more calcium and magnesium may explain the higher concentrations of NO_3^- in coarse mode and also the higher temperature may reduce the concentrations of NO_3^- in fine mode. Na^+, Cl^- and K^+ exhibited bimodal size distributions; Ca^{2+} and Mg^{2+} showed maximum values in coarse mode. Aerosol acidity analysis showed a higher acidity of aerosol particles at LL when compared with those at SM. The average concentration of $[H^+]$ was relatively low when compared with those observed at two other mountains in China. This corresponds with the relatively low concentrations of SO_4^{2-} and HSO_4^- and lower water content at Huangshan.

1. Introduction

Atmospheric aerosols play a crucial role in global climate by directly affecting earth's radiative balance and indirectly altering cloud-precipitation properties by acting as cloud condensation nuclei (CCN) or ice nuclei (IN). They can also raise adverse impacts on human health and the atmospheric environment (Vedal et al., 2009). These effects are associated with their physical and chemical properties. The chemical compositions of aerosol particles determine their hygroscopicity and solubility and thus the size changes with relative humidity (RH) increased and it also influence the optical properties of aerosol (Henning et al., 2003). Ma et al. (2012) also shows that the hygroscopicity of aerosol particles is mainly determined by the water-soluble compositions and amount

* Corresponding author. School of Atmospheric Physics, Nanjing University of Information Science and Technology, Ningliu Road 219, Nanjing, China.
E-mail addresses: yinyan@nuist.edu.cn, yyatnuist@yahoo.co.uk (Y. Yin).

http://dx.doi.org/10.1016/j.atmosenv.2014.08.077
1352-2310/

of inorganic salts in them. Particles could act as CCN even if they contained only quite a small amount (~5%) of highly soluble substances (Andreae and Rosenfeld, 2008). Sulfate and organic matter were the main chemical components contributed to light extinction and visibility degradation (Liu et al., 2008). Previous studies found that water-soluble inorganic ions (WSI) are the main components of aerosols, especially for fine particles. Therefore, it is scientifically important to investigate the WSI properties for full understanding aerosols' physical and chemical characteristics, sources, behavior and formation mechanisms.

Numerous studies on WSI have conducted in many areas of China, but most of them were carried out in urban regions (e.g., Wang et al., 2005; Cao et al., 2009; Shen et al., 2009; Cheng et al., 2011; Zhang et al., 2011; Zhao et al., 2011). It should be emphasized that the ground-based results are not entirely representative to the physical and chemical properties of aerosol particles at upper levels or in the free troposphere, where aerosols are more likely to be transported for a long distance or more directly acted as CCN (Li et al., 2011a). Moreover, the vertical distribution of aerosol components suggests complex profiles, which depends on the variation of atmospheric stability and temperature inversions (Chan et al., 2005). Up to date, studies on size and vertical distributions of aerosols at mountainous sites are still inadequate. Previous studies related to the vertical distribution of WSI in China were mostly conducted at meteorological towers or buildings lower than 300 m (Tian et al., 2013), where the characteristics of aerosols in atmospheric boundary layer are not able to be fully represented. Therefore, better understanding of the distribution and formation mechanisms of atmospheric ionic species at the top of the boundary layer is required, and this can be achieved via the measurements at high mountainous sites.

Numerous studies have been conducted at mountainous sites, such as Jungfraujoch (Henning et al., 2003), Mountain Lulin (Lee et al., 2011), Mt. Oyama (Takeuchi et al., 2004), Mount Hua (Rosenfeld et al., 2007; Li et al., 2011a; Wang et al., 2011), Mount Tai (Wang et al., 2009; Zhou et al., 2009; Deng et al., 2011; Li et al., 2011b; Wang et al., 2011, 2012a, 2012b), Mount Heng (Gao et al., 2012) and Mount Lu (Li et al., 2013, 2014). These studies however have mainly focused on the summit sites, very few studies have considered the diversity of aerosols and their chemical compositions at different altitudes of the mountains. To fill this gap, we conducted a field campaign at the summit and a lower height of Huangshan, the continental background site for southeast China. This study is part of a project to investigate the changes in physical and chemical properties of atmospheric aerosols and cloud droplets and their interactions in southern mountainous area of China funded by China National Natural Science Foundation (Chen et al., 2014). The main objectives of this study are: (1) to investigate the mass concentrations of particles and WSI at a mountainous background site in southeast China; (2) to investigate the size distribution patterns, potential sources and formation processes of WSI; (3) to analyze the vertical distribution of aerosols and ions at different altitudes.

2. Methodology

2.1. Field experiments

The experiment was conducted at two altitudes simultaneously. The summit sampling site (SM) was set at the meteorological station of BrightPeak (30.13°N, 118.15°E, 1840 m a.s.l.). The other site was located at a lower level of Huangshan (LL) (30.12°N, 118.19°E, 869 m a.s.l). Huangshan locates at the southwest of Yangtze River Delta region of China which is a tourist region with few industrial activities. The campaign was performed from 14 September to 26 October, 2012. Aerosol particles with size ranges of 10.0–9.0, 9.0–5.8, 5.8–4.7, 4.7–3.3, 3.3–2.1, 2.1–1.1, 1.1–0.65, 0.65–0.43 and <0.43 μm were collected with two Anderson-type particle samplers (Anderson 2000 Inc., USA), operating at a constant flow rate of 28.3 L/min. The size-segregated aerosol particles were continuously collected for 24 h at each site with Teflon filters (pore size as 0.22 μm, Xingya Ltd., Shanghai, China). Totally 27 and 24 sets of filters were obtained for the SM and LL site, respectively.

2.2. Ion analysis

The filters were weighted after balanced at a constant temperature (25 °C) and relative humidity (50%) for 48 h before and after sampling. They were then stored in a refrigerator under −20 °C before ionic analysis. An 850 professional Ion chromatography (Switzerland, 850 professional IC, Metrohm) was used to analyze WSI. Half of each Teflon filter was cut and placed into a 20 mL PET vial, ultrasonically extracted for 0.5 h and mechanically oscillated for 1 h with 10 mL deionized water (18.2 MΩ). PTFE filters were used to remove the insoluble particles and filter chips in the extraction prior to analysis by IC. Eight ions including Cl^-, NO_3^-, SO_4^{2-}, Na^+, NH_4^+, Mg^{2+}, K^+ and Ca^{2+} were analyzed. Anions were detected by Metrosep A Supp 5-150/4.0 separation column with 3.2 mmol/L Na_2CO_3 + 1.0 mmol/L $NaHCO_3$ as eluent. Cation separation column was Metrosep C4-150/4.0, and the cation eluent was 1.7 mmol/L HNO_3 + 0.7 mmol/L pyridine carboxylic acid. The detection limits for Cl^-, NO_3^-, SO_4^{2-}, Na^+, NH_4^+, K^+, Mg^{2+} and Ca^{2+} were 0.01, 0.01, 0.01, 0.001, 0.005, 0.001, 0.001 and 0.001 mg/L, respectively. Detailed information can refer to our previous study (Kong et al., 2014).

2.3. Meteorological conditions and backward trajectory calculations

Meteorological parameters were obtained by two automatic weather stations (Vantage Pro2, Davis, USA). Fig. 1 shows the time series of meteorological parameters at the two sites of Huangshan during the experimental period. The average temperature during the campaign was 10.7 °C and 16.7 °C for SM and LL, respectively. The average relative humidity (RH) was 64.5% and 69.4% at SM and LL, and the diurnal variation of RH at SM was more dramatic than that at LL. The wind speed at SM (4.55 m/s) was 10 times higher than that at LL (0.43 m/s) with obvious diurnal variation. 72 h air mass backward trajectories were calculated terminating at the height of 1480 m (the height of SM above ground base) by using the Hybrid Single Particle Lagrangian Integrated Trajectory model (HYSPLIT) with the Global Data Assimilation system (GDAS) data as meteorological inputs.

2.4. Thermodynamic model

Aerosol acidity plays an important role in aerosol phase reactions. It can catalyze many heterogeneous atmospheric chemical processes between the gas phase and particle surfaces to enhance the formation of secondary inorganic aerosols (Yao et al., 2006; Manktelow et al., 2010). In situ aerosol acidity (H^+_{air}) is defined as the moles of free hydrogen ions in the aqueous phase of aerosols per unit volume of air (nmol/m^3). However, H^+_{air} is difficult to measure directly since the amount of aqueous water in aerosol is very small. In this study, the online version of chemical thermodynamic model (Aerosol Inorganic Model: AIM-II) (http://www.aim.env.uea.ac.uk/aim/aim.htm) was used to investigate the acidic characteristics of $PM_{2.1}$. Several studies have reported that AIM-II can accurately evaluate the acidity characteristics of aerosols (Pathak et al., 2003; Yao et al., 2006; Cheng et al., 2011). The average

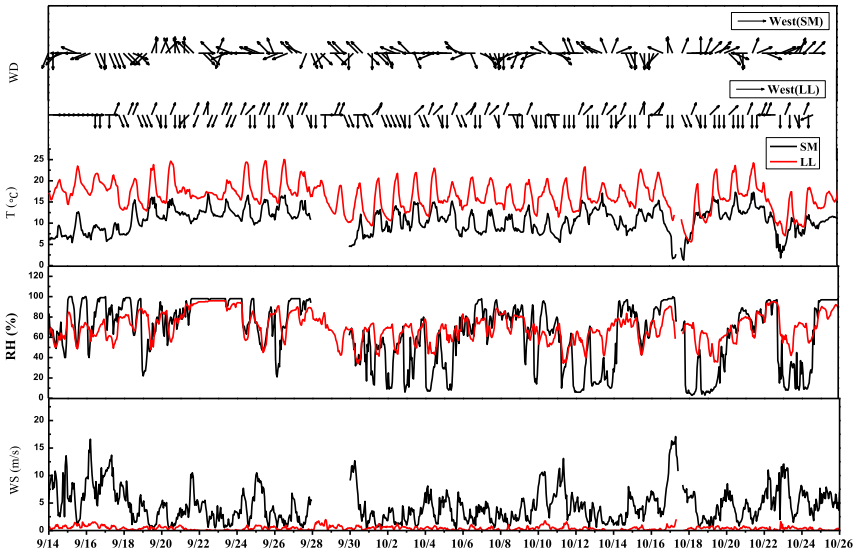

Fig. 1. Time series of meteorological parameters at Huangshan during the study period.

ambient temperature, relative humidity, and the concentrations of SO_4^{2-}, NO_3^-, NH_4^+ and the calculated H^+_{strong} were used as inputs of the model. Strong acidity (H^+_{strong}), defined as $[H^+]_{strong} = 2 \times [SO_4^{2-}] + [NO_3^-] - [NH_4^+]$, includes the total amount of acid contributed by the strong acids, such as hydrogen ion released from sulfuric and/or nitric acid and the actual free hydrogen ion (H^+_{air}) in the aqueous phase of aerosols. The aqueous phase concentrations of in situ acidity (H^+_{air}), bisulfate (HSO_4^-), SO_4^{2-}, NO_3^- and water content in the aerosol droplets can be obtained. The in situ pH of aerosols was predicted by the mole concentrations of the free hydrogen ion in the aqueous phase of particle droplets, using the equation (Zhou et al., 2012).

$$pH = -\log\left[\gamma \times \left[H^+\right]_{air} \Big/ (V_{aq}/1000)\right] \quad (1)$$

Where γ is the activity coefficient of H^+_{air} (mol/m^3) and V_{aq} denotes the volume of particle aqueous phase in air (cm^3/m^3).

3. Results and discussion

3.1. Mass concentrations

3.1.1. Mass concentrations of aerosols at different altitudes

Since there is no cut-point of Andersen sampler for particles of 2.5 μm in diameter, the cut point of 2.1 μm is used to divide PM_{10} into $PM_{2.1}$ (fine particles) and $PM_{2.1-10}$ (coarse particles). Table 1 summarizes the average mass concentrations of PM_{10}, $PM_{2.1}$ and $PM_{1.1}$, as well as WSI in them at SM and LL sites. The PM_{10} mass concentrations ranged from 7.10 to 79.73 μg/m^3 at SM and from 12.13 to 72.90 μg/m^3 at LL, with the average and standard deviation values of 39.25 ± 15.17 μg/m^3 (SM) and 42.39 ± 15.93 μg/m^3 (LL). The concentration of PM_{10} at LL was 8% higher than that at SM. The $PM_{2.1}$ concentrations were in the ranges of 4.93–44.27 and 11.57–59.42 μg/m^3 at SM and LL site, respectively. At LL it was 36% higher than that at SM. For submicron particle ($PM_{1.1}$), they ranged from 4.93 to 33.07 μg/m^3 at SM and from 9.63 to 51.30 μg/m^3 at LL (45% higher than that at SM). It indicated that the particle concentrations decreased with the altitude increasing, and the vertical variation is more obvious for finer particles.

The average mass concentrations of total WSI in PM_{10} were 17.16 and 27.61 μg/m^3 at SM and LL, and were 11.73 and 19.38 μg/m^3 for $PM_{2.1}$, respectively. The average mass percentages of WSI at LL were higher than those at SM. The total WSI accounted for 55.71% (SM) and 64.76% (LL) of $PM_{1.1}$, higher than those for $PM_{2.1}$ and PM_{10}, implying that they accumulated in finer particles more easily. The total amounts of secondary ions ($SO_4^{2-} + NO_3^- + NH_4^+$) accounted for 59.39% and 70.96% of the total WSI in PM_{10} and $PM_{2.1}$ at SM. And the corresponding percentages were higher at the LL site. It can be concluded that the ions were dominated by SO_4^{2-}, NO_3^- and NH_4^+ at both sites and more secondary ions could be formed at the lower site LL. However, the percentages of total amount of secondary ions in $PM_{1.1}$ increased with increasing altitude. It is related to the fact that the concentrations of NO_3^- in submicron particles at LL were lower than that at SM, which will be further discussed in the following sections.

Table 1
Average mass concentrations of PM_{10}, $PM_{2.1}$ and $PM_{1.1}$ and ions at different altitudes of Huangshan (μg/m^3).

Location	Particle size	Mass concentrations		TI/PM (%)	($SO_4^{2-} + NO_3^- + NH_4^+$)/TI (%)
		Particles	Total ions (TI)		
SM	PM_{10}	39.25	17.16	43.18	59.39
	$PM_{2.1}$	21.28	11.73	55.50	70.96
	$PM_{1.1}$	17.07	9.59	55.71	74.18
LL	PM_{10}	42.39	27.61	60.22	66.09
	$PM_{2.1}$	29.02	19.38	61.72	77.52
	$PM_{1.1}$	24.79	16.88	64.76	59.64

TI: sum of water soluble inorganic ions.

3.1.2. Mass concentrations of ions

Fig. 2 shows the characteristics of WSI at the two sampling sites. For the coarse particles at SM, Ca^{2+}, with the mass concentration of 1.93 μg/m^3, contributed the largest fraction (39%) of the total WSI, followed by NO_3^- (0.96 μg/m^3) and SO_4^{2-} (0.72 μg/m^3), accounting for 19% and 14%, respectively. Na^+ and Cl^-, which are related to sea-salt, totally account for 10% of WSI in coarse particles. The mass concentrations of WSI in fine particles at SM excited decreasing trend in the order of SO_4^{2-} (5.54 μg/m^3) > NH_4^+ (2.24 μg/m^3) > Ca^{2+} (1.34 μg/m^3) > NO_3^- (0.99 μg/m^3). The order of WSI species in $PM_{1.1}$ was similar to that in $PM_{2.1}$. But SO_4^{2-} and NH_4^+ accounted for 51% and 22% of ions in $PM_{1.1}$, higher than those of 48% and 19% in $PM_{2.1}$.

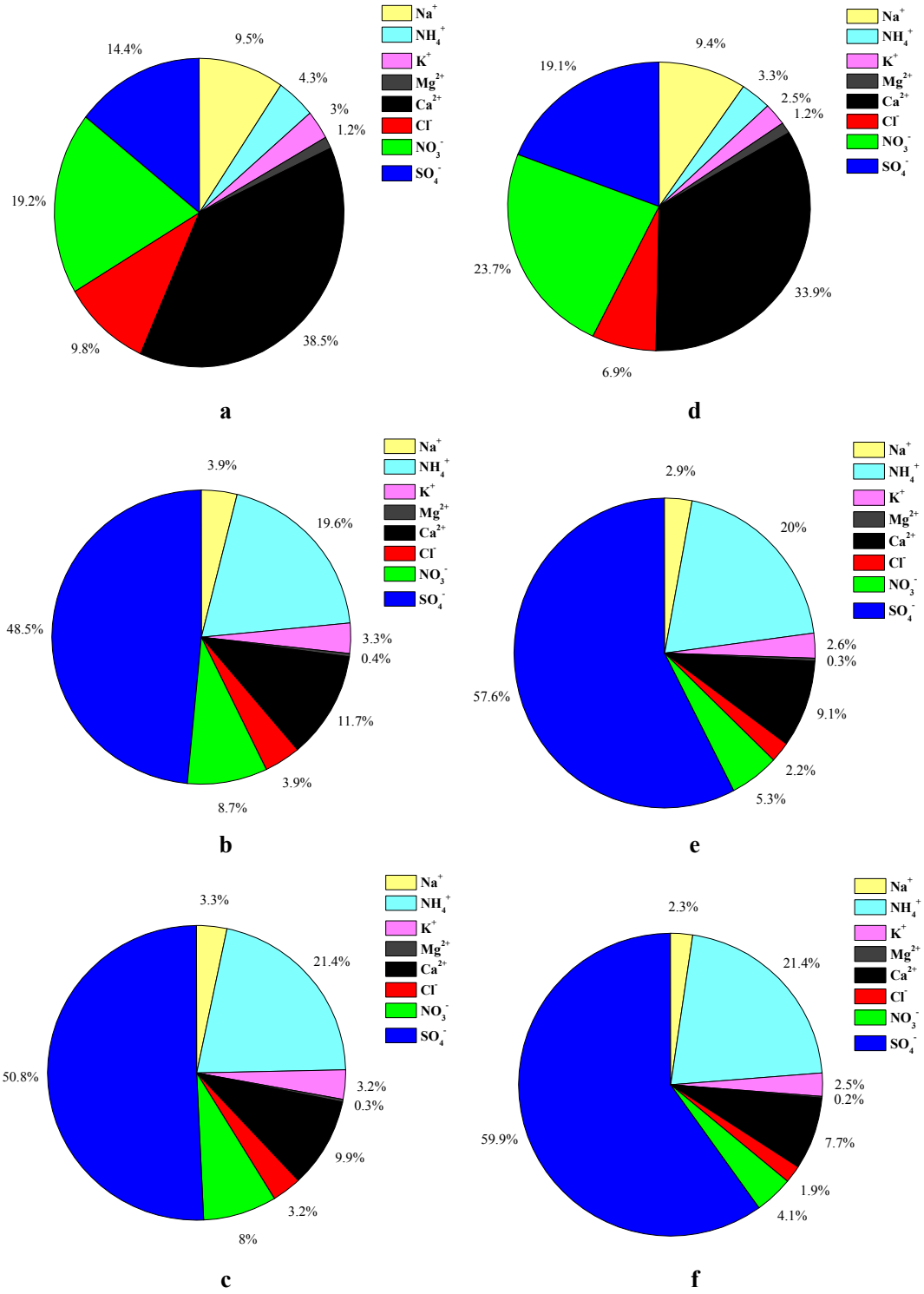

Fig. 2. Characteristics of the water-soluble inorganic ions at the two sampling sites. a, b, c are corresponding to $PM_{2.1-10}$, $PM_{2.1}$, $PM_{1.1}$ at SM; d, e, f are corresponding to $PM_{2.1-10}$, $PM_{2.1}$, $PM_{1.1}$ at LL, respectively.

The mass percentage of WSI at LL was consistent with that at SM. Whereas, the mass concentrations of most ions in $PM_{2.1-10}$, $PM_{2.1}$ and $PM_{1.1}$ at LL were 1–2 times of the corresponding ones at SM, except for Cl^- in $PM_{2.1}$ and NO_3^- in $PM_{1.1}$. Several studies reported that mountain valley breezes and convective mixing within the planetary boundary layer (PBL) have a great impact on the concentrations of aerosol particles at mountain sites (Li et al., 2011b; Gao et al., 2012). In this study, the average mass concentrations of particulate matter, total WSI and each ion all decreased with increasing altitude. These may be explained as: (1) the atmosphere at SM is cleaner than that at LL where anthropological activities are intensive; (2) polluted air masses could be transported from the ground to the mountain top by upslope winds along the mountain slopes and by the uplifting PBL in the daytime. Aerosols

could lose through dry or wet deposition processes and the dilution effects during transportation processes. The pollutants from lower levels can be removed during transport to the summit which may also lead to the decrease of aerosol particles and ions. The different sources for particles at SM and LL from principal component analysis (Table 2) can also verify the differences between them. For PM_{10} at SM and LL, 78% and 77% of the total variance were extracted. For SM, factor 1 accounting for 38% of the total variance, with high loadings of K^+ and SO_4^{2-}, indicating the influence of biomass burning and its aging courses; Factor 2, accounting for 26%, was dominated by Na^+ and Cl^-, and thus was attributed to the sea salt; Factor 3 presented a high loadings of NO_3^- and Mg^{2+}, suggesting that it is related with the heterogeneous reaction of nitrate gaseous precursors with aerosols containing Mg^{2+}. For LL, high loadings for NH_4^+ and SO_4^{2-} in factor 1 suggested the dominant role of secondary reactions (accounting for 30%); Factor 2 showed high loadings of Na^+, K^+, Ca^{2+} and NO_3^-, and thus was attributed to the crustal materials and sea salt and the heterogeneous reaction of nitrate gaseous precursors on them. It can be found that the contributions of anthropological sources (for secondary ions) and crustal materials were higher at LL which can also explain the higher concentrations of aerosols and ions at this site.

3.2. Size distribution of ions

The chemical properties, lifetime and sources of aerosol particles can be revealed by size distribution of chemical compositions. The concentrations of ions in size-segregated particles are shown in Fig. 3.

3.2.1. Sulphate, ammonium and nitrate

The size distribution of sulfate at SM exhibited bimodal, peaking at the size ranges of 0.43–0.65 μm and 4.7–5.8 μm, respectively, but exhibited tri-modal with the major peak at 0.65–1.1 μm for LL, suggesting more complex sources of sulfate at LL. The formation of sulfate aerosol is mainly driven by the oxidation of precursors to gaseous H_2SO_4, followed by nucleation and condensation processes (Andreae and Rosenfeld, 2008). Sulfate at SM was dominant at 0.43–0.65 μm, whereas at LL the sulphate peaks at 0.65–1.1 μm. High temperature, strong sunlight in daytime at SM favored the heterogeneous condensation of SO_2 and H_2SO_4 to form particles. Gao et al. (2012) indicated that in-cloud process was the dominant pathway for larger particles, which was formed by the oxidation of SO_2 in cloud droplets. However, there was little cloud or fog processes at LL during the sampling period, thus the relatively high RH played a principal role in formation of sulfate in larger particles at LL. The diurnal variation of RH was moderate so that RH kept a high value at LL. Increased water uptake onto the aerosol particles can lead aerosols growing into larger size hereby the major fractions shifted to a larger mode. Sulfate in coarse particles can be contributed by sea-salt and secondary sulfate that was mainly produced through reactions of SO_2 or gaseous H_2SO_4 on the pre-existing large particles (Zhao and Gao, 2008). Table 3 shows the good correlations between SO_4^{2-} and K^+ in coarse mode, indicating they may have same sources in coarse particles.

Ammonia vapor (NH_3) could form fine particulate ammonium through reactions with acidic particles and the conversion depends on the acidic species, temperature and humidity in the atmosphere (Liu et al., 2008; Zhang et al., 2011). Among the products of NH_3 through gas-phase or aqueous-phase reactions with acidic species, $(NH_4)_2SO_4$ is preferentially formed and is the least volatile species; NH_4NO_3 is formed next and NH_4Cl is the last (Zhang et al., 2008). Previous studies indicated that the formation and size distributions of SO_4^{2-} and NO_3^- depends on the concentration of NH_4^+, whether ammonia-rich or ammonia-poor, and were related to the presence of coarse particles (Liu et al., 2008). The mass size distribution of ammonium was in accordance with that of sulfate which presented a similar bimodal pattern at both sites, with most fractions (>90%) existing in fine particles. At SM, NH_4^+ in the range of 0.43–0.65 μm dominated and at LL, it was dominated at the range of 0.65–1 μm, indicating that NH_4^+ was mainly formed through the gas-to-particle condensation reactions at SM, while in-cloud process played a principal role at LL. This could be owing to the differences in meteorological conditions as discussed above.

The contributions of various pathways of nitrate formation to $PM_{2.1}$ mass are less known compared to the formation of sulfate (Pathak et al., 2009). Typically, NO_3^- in fine mode was generated by the gas-to-particle conversion, whereas NO_3^- in coarse mode was mainly formed through heterogeneous condensation of nitric acid onto the surfaces of the existing coarse particles. In this work, there was obvious discrepancy of size distributions for nitrate between SM and LL. Nitrate showed a bimodal distribution at SM with a dominant peak in the size range of 0.43–0.65 μm and a peak in the coarse mode. In contrast, at LL, it mainly existed in the coarse mode (65% existed in $PM_{2.1-10}$). It suggested the formation mechanism of nitrate is different at SM and LL. To investigate the nitrate formation mechanism at different altitudes of Huangshan, we examine the relationship of sulfate, nitrate and ammonium in more detail.

The equivalent of nitrate plus sulfate to ammonium is shown in Fig. 4 which was used to evaluate the acidic characteristics of $PM_{2.1}$. At LL, higher concentrations of sulfate and nitrate were shown and the ratio was higher than one, indicating that acidic aerosols were only partially neutralized by ammonium. Thus, the aerosols were ammonium-poor. In contrast, the ratio close to one at SM indicated that a complete neutralization of sulfate and nitrate was almost

Table 2
Factor loadings from principal component analysis.

Species	SM			LL	
	Factor 1	Factor 2	Factor 3	Factor 1	Factor 2
Na^+	0.550	**0.741**	−0.105	−0.327	**0.832**
NH_4^+	0.696	−0.646	−0.264	**0.864**	0.426
K^+	**0.909**	0.125	−0.133	0.459	0.614
Mg^{2+}	0.540	−0.048	**0.563**	−0.331	**0.877**
Ca^{2+}	0.615	0.570	−0.045	−0.390	**0.763**
Cl^-	0.079	**0.649**	−0.263	−0.658	0.574
NO_3^-	0.448	−0.043	**0.728**	0.211	**0.674**
SO_4^{2-}	**0.724**	−0.591	−0.303	**0.770**	0.581
Of variance	38%	26%	14%	30%	47%
Sources	BB and its aging courses	Sea salt	Heterogeneous reaction on crustal materials	Secondary reactions	Crustal materials/sea salt and heterogeneous reaction on them

The two species with higher loadings for each factor were shown in bold.

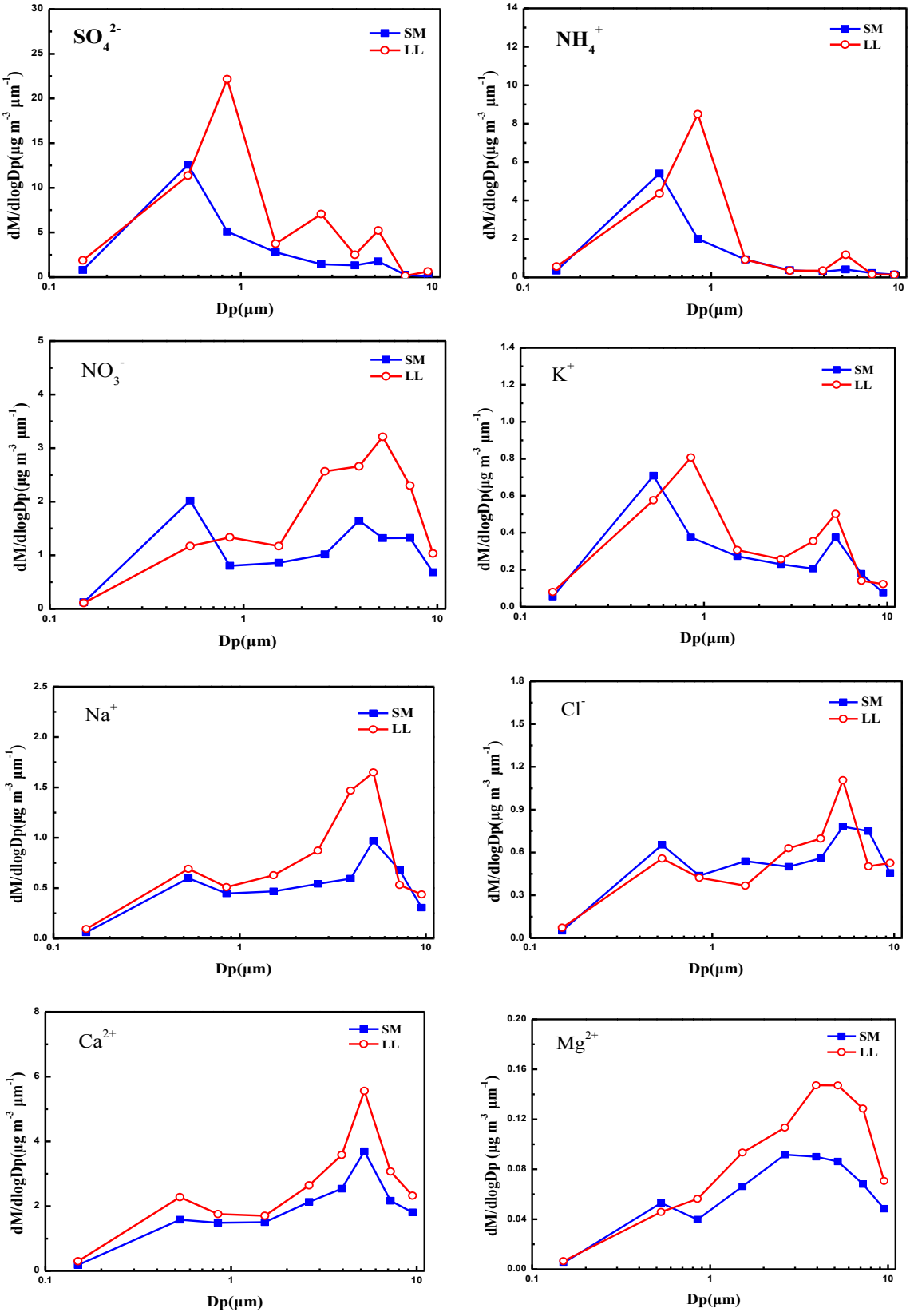

Fig. 3. Size distribution of main water-soluble inorganic ions at SM and LL.

Table 3
Pearson correlation coefficients for major ions in different size-ranges of aerosols at SM and LL of Huangshan.

	D_p < 0.43 μm		0.43μm < D_p < 0.65 μm		0.65μm < D_p < 1.1 μm		1.1μm < D_p < 2.1 μm		2.1 μm < D_p < 10 μm	
SO_4^{2+}–NH_4^+	SM	0.953[a]	SM	0.974[a]	SM	0.982[a]	SM	0.952[a]	SM	0.711[a]
	LL	0.319	LL	0.990[a]	LL	0.997[a]	LL	0.916[a]	LL	0.237
NO_3^-–Ca^{2+}	SM	0.203	SM	0.253	SM	0.040	SM	0.227	SM	0.462[b]
	LL	−0.137	LL	−0.349	LL	−0.044	LL	0.216	LL	0.469[b]
NO_3^-–Mg^{2+}	SM	0.281	SM	0.087	SM	0.128	SM	0.153	SM	0.460[b]
	LL	−0.246	LL	0.248	LL	0.047	LL	0.727[a]	LL	0.681[a]
Na^+–Cl^-	SM	−0.007	SM	0.404[b]	SM	0.045	SM	0.244	SM	0.605[a]
	LL	0.785[a]	LL	0.558[a]	LL	0.483[b]	LL	0.618[a]	LL	0.584[a]
K^+–Na^+	SM	0.382[b]	SM	0.329	SM	0.272	SM	0.737[a]	SM	0.899[a]
	LL	0.513[b]	LL	0.725[a]	LL	0.334	LL	0.431[b]	LL	0.673[a]
K^+–Cl^-	SM	0.060	SM	0.029	SM	−0.085	SM	0.551[a]	SM	0.517[a]
	LL	0.636[a]	LL	0.322	LL	0.107	LL	0.208	LL	0.216
SO_4^{2-}–K^+	SM	0.709[a]	SM	0.469[a]	SM	0.501[a]	SM	0.354	SM	0.524[a]
	LL	0.335	LL	0.368	LL	0.703[a]	LL	0.524[a]	LL	0.407[b]
Mg^{2+}–Na^+	SM	0.181	SM	0.598[a]	SM	0.465[b]	SM	0.433[a]	SM	0.045
	LL	0.340	LL	0.128	LL	0.359	LL	0.861[a]	LL	0.713[a]
Ca^{2+}–Na^+	SM	0.551[a]	SM	0.644[a]	SM	0.627[a]	SM	0.285	SM	0.551[a]
	LL	0.402	LL	0.536[a]	LL	0.528[a]	LL	0.618[a]	LL	0.478[b]

[a] Correlation is significant at the 0.01 level (2-tailed).
[b] Correlation is significant at the 0.05 level (2-tailed).

achieved and these samples were ammonium-rich. The samples at Mt. Hua were ammonium-poor with high acidity degree whereas those were ammonium-rich at Mt. Tai as the relatively abundant NH_3 existed (Wang et al., 2011).

Fig. 5a depicts the normalized nitrate concentration (mole of nitrate per mole of sulfate) as a function of normalized ammonium concentration (mole of ammonium per mole of sulfate). These ratios are used to show the reactions between ammonia and nitric acid and the other formation processes of nitrate in different (relative) concentrations of sulfate (Pathak et al., 2009). As shown in Fig. 5a, the ammonium-rich and poor are defined with a threshold of 2: ammonium-rich ($NH_4^+/SO_4^{2-} > 2$) and ammonium-poor ($NH_4^+/SO_4^{2-} < 2$). The normalized nitrate concentration increased as the ratio of ammonium to sulfate increased from two. In this study, "excess ammonium" is defined as $[NH_4^+] = ([NH_4^+]/[SO_4^{2-}] - 2) \times [SO_4^{2-}]$). Fig. 5b shows the concentration of nitrate as a function of excess ammonium. The concentration of nitrate increased with increasing excess ammonium, implying that in the ammonium-rich samples, nitrate or the nitrate-sulfate salts of ammonium formed via the gas-phase homogeneous reaction by the following pathway: $NH_3 + HNO_3 \rightleftarrows NH_4NO_3$. As shown in Fig. 5a, there were 44% and 32%, respectively, of the samples at SM and LL existed in the ammonium-rich region, implying that larger fraction of nitrate at SM in $PM_{2.1}$ were formed via the gas-phase homogeneous reactions. Therefore the mass percentages of nitrate in fine mode of the total nitrate mass at SM (51%) were higher than that for LL (35%). It should be noted that 32% samples at LL existed in the ammonium-rich region indicating that the homogeneous gas-phase reactions may occur at LL, but no peak of nitrate presented in the fine mode. It might be caused by the higher temperature which reduced the formation of nitrate in accumulation mode, and may increase the thermal volatilization hereby decreasing the nitrate collection efficiency. Zhao and Gao (2008) observed that the fractions of nitrate in fine particles showed a negative correlation with temperature and they found 17 °C was likely to be a critical point of the transformation for the dominant nitrate fractions between fine and coarse mode. In this study, the percentages of NO_3^- was lower than 0.1 when the temperature at LL was higher than 17 °C (Fig. 6), while it increased when temperature below 17 °C. During the campaign, diurnal average temperatures at SM were always lower than 17 °C, and the corresponding percentages of nitrate were higher than those of LL. The lower ambient temperature was observed to favor the formation of NH_4NO_3 (Cao et al., 2009).

The ratios of NO_3^-/SO_4^{2-} were scattered when $[NH_4^+]/[SO_4^{2-}] < 2$ for the samples at SM and LL (Fig. 5a). The normalized nitrate concentration decreased as the normalized ammonium increased, thus the nitrate formation in these samples may not be explained by the homogeneous gas-phase mechanism. Pathak et al. (2009) found that the nighttime heterogeneous hydrolysis of N_2O_5 on the moist surface of the pre-existing aerosols was responsible for the formation of the observed nitrate. In the ammonium-poor region, the combination of NH_4^+ and SO_4^{2-} was mainly in the form of NH_4HSO_4, which indicated that the sulphate was not neutralized completely by ammonium, and thus there was not enough ammonium to neutralize the nitric acid. The gaseous precursor of nitrate could react with coarse particles containing alkaline species like Na, Ca, Mg and K, and the productions in coarse mode was easier to be sampled. As shown in Table 3, at both sites, NO_3^- showed good correlations with Mg^{2+} and Ca^{2+} in coarse mode with

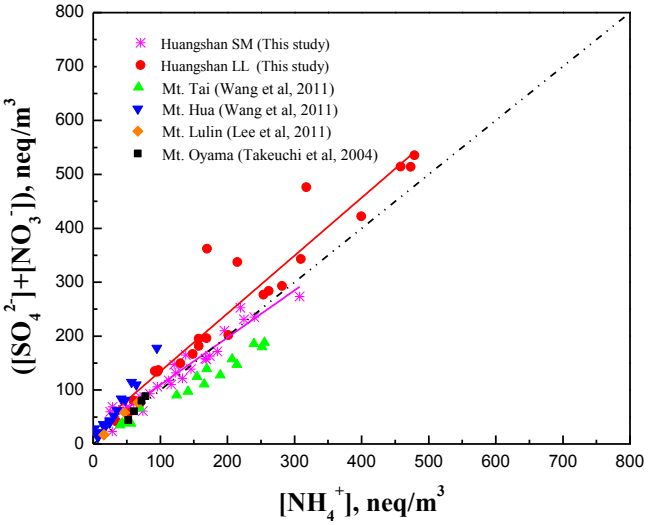

Fig. 4. Sum of sulfate and nitrate as a function of ammonium equivalent concentrations in $PM_{2.1}$.

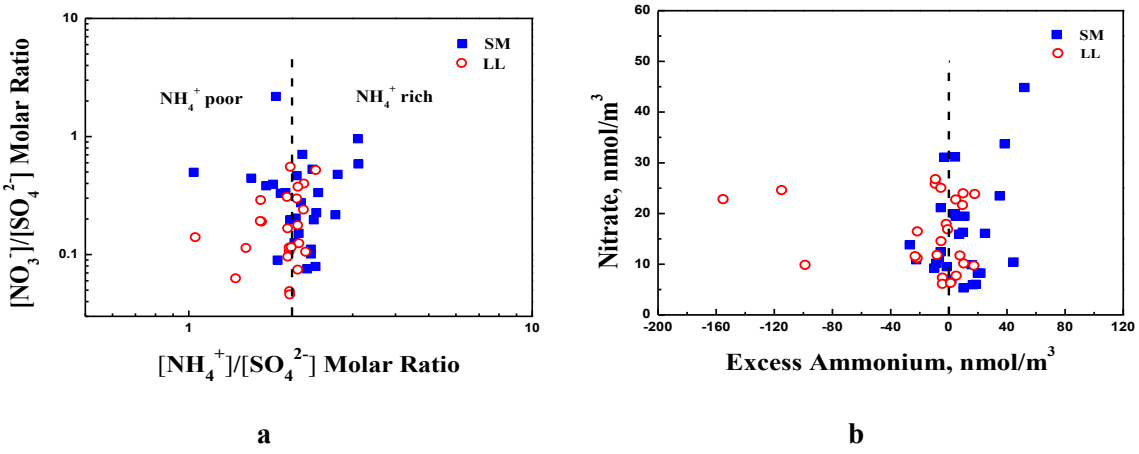

Fig. 5. (a) Nitrate to sulfate molar ratio as a function of ammonium to sulfate molar ratio; (b) Nitrate concentration as a function of Excess Ammonium.

correlation coefficient (R) of 0.68 for NO_3^-–Mg^{2+} and 0.47 for NO_3^-–Ca^{2+} at LL, respectively. It suggested that the major source of particulate nitrate in coarse mode was the reaction of gaseous HNO_3 on the surface of coarse particles or precursor gases reacted with marine and crustal species through the heterogeneous condensation. The transmission electron microscopy observations at Mt. Lu showed that mineral particles are mainly covered with coatings including $Mg(NO_3)_2$ and $Ca(NO_3)_2$, and these coatings enhance both the size and hygroscopic properties of mineral particles (Li et al. 2011a, b). These reactions could explain the abundant of Ca^{2+} at coarse particles as shown in Fig. 2.

3.2.2. Potassium

Bimodal size distributions of K^+ were obtained at both sites, peaking in both fine and coarse mode. K^+ has multiple sources, including soil-derived, vegetation burning and sea-salt (Zhang et al., 2008). K^+ in fine particles can serve as a diagnostic tracer for biomass burning (BB) (Andreae et al., 1998). Fig. 7 shows the fire points of field BB around Huangshan and 72 h back trajectories of the air masses arriving SM from 23 September to 2 October. Back trajectories presented that the air masses mainly came from two directions. On 23–26 September, the air masses arriving SM were transported from East China Sea (sea case), which would carry some BB species but considerable sea-salt. During this period, the size distribution of K^+ showed obvious peaks in coarse mode, accounting for 38% of K^+ in PM_{10}, and high positive correlation between K^+ and Na^+ in coarse mode at both sites was found suggesting the sea-salt was the major source for K^+ in coarse mode. From 29 September to 2 October, the origin of air masses shifted to the north (north case), bringing abundant species emitted from BB. The fraction of K^+ is only 17% in coarse mode, with 83% in fine mode, indicating that K^+ in fine mode was mainly influenced by BB. Pearson correlation coefficients showed that the mass concentrations of potassium and sulfate exhibited a strong correlation in fine mode (Table 3). Here we can presume that the particles from BB carried sulfate into Huangshan. This is in agreement with the study at Mt. Lu where certain amounts of potassium salts coexisted in secondary sulfate particles (Li et al., 2014). The mass ratio of Cl^-/K^+ was 1.41 and 0.70, and the concentrations of Cl^- were 0.89 and 0.69 μg/m^3 in the sea case and the north case, respectively. Wang et al. (2011) found that KCl salt in fresh BB smoke can be readily converted into K_2SO_4 and KNO_3 during the smoke aging process by reacting with acid gases. The KCl salt emitted by BB at Huangshan may have reacted with H_2SO_4 and release HCl, and led to the lower mass ratio of Cl^-/K^+ in the north case than that for the sea case.

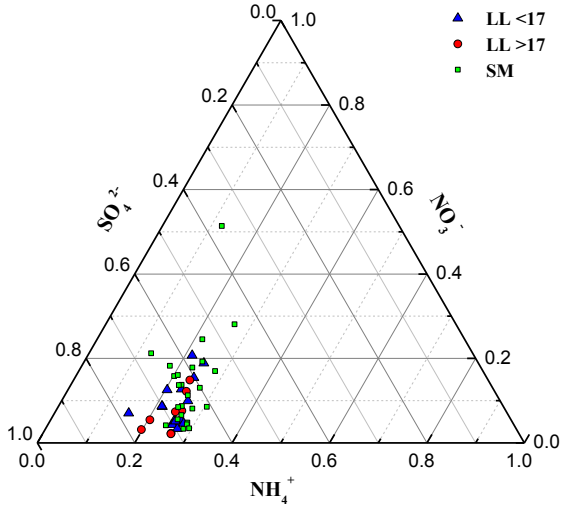

Fig. 6. Ternary diagram for the ratio of sulfate, nitrate and ammonium.

3.2.3. Calcium, magnesium, chloride and sodium

Ca^{2+} and Mg^{2+} tend to accumulate in coarse mode because they were mainly from soil particles or dust. In addition, sea-salt could be a contributor to Mg^{2+} for coarse fractions (Zhao et al., 2011). This is supported by the tight correlation between Na^+ and Mg^{2+} (1.1–10 μm). Bimodal distribution of Na^+ and Cl^- could be found at both sites, but the major fraction of Na^+ was in coarse mode and two considerable peaks of Cl^- were in fine and coarse mode. The good correlations between Na^+ and Cl^- in both fine and coarse modes suggested that there were similar origins of Na^+ and Cl^- at Huangshan. One was sea-salt for Na^+ and Cl^- in coarse mode and the other for Na^+ and Cl^- in accumulative mode might come from anthropogenic emissions, such as waste incineration (Zhao et al., 2011). Several studies found that vegetation fire emissions were Cl^- enriched and almost released in particle phase (Andreae et al., 1998; Wang et al., 2011). In fine particles the concentration of Cl^- was 7.8% higher at SM than that at LL. The reason might be attributed to that the particle Cl^- from long-range transport to SM increased the loadings of Cl^- in the fine mode.

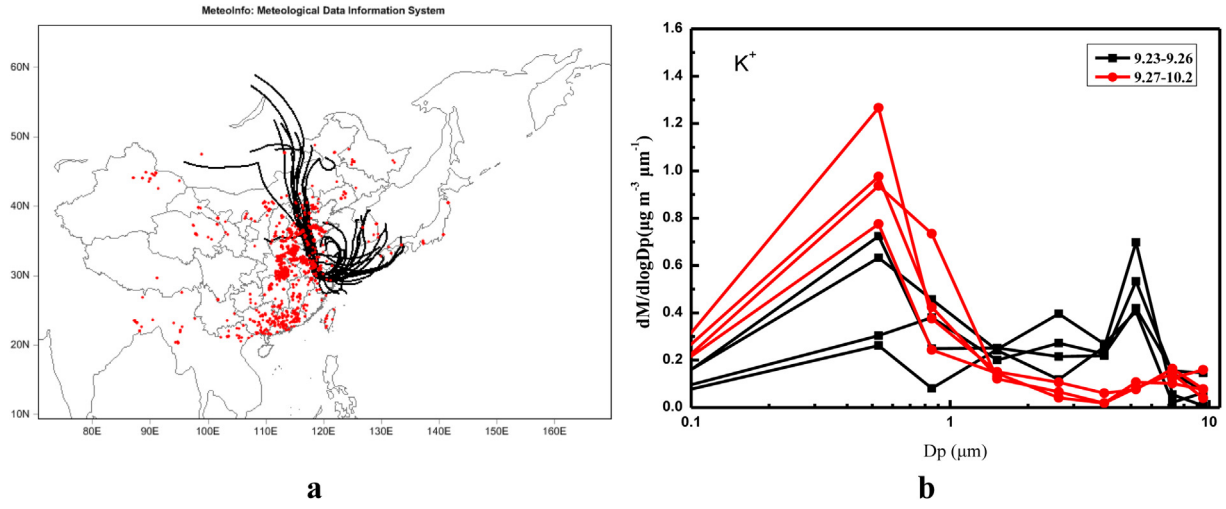

Fig. 7. (a) Fire points and backward trajectories during 9.23–10.2; (b) Size distributions of K^+ during 9.23–10.2 at SM.

Table 4
Comparison of aerosol acidity of $PM_{2.1}$ at Huangshan and other mountainous sites in China.

Location	Season	$[H^+]_{strong}$ nmol/m^3	$[H^+]_{air}$ nmol/m^3	HSO_4^- nmol/m^3	pH	Water content ug/m^3	Reference
Hungshan (SM)	Autumn	19.08	5.78	13.3	0.41	9.98	This study
Hungshan (LL)	Autumn	36.10	6.96	32	0.29	9.49	
Mt. Heng	Spring	53.4	13.3	35.6	0.64	67.7	Gao et al., 2012
Mt. Tai	Spring	64.82	25.25	67.66	−0.32	47.89	Zhou et al., 2012
Mt. Tai	Summer	142.65	35.27	121.34	−0.04	78.57	

3.3. *Aerosol acidity and water content*

Aerosol acidity plays a crucial role in secondary aerosol formation and also influences aerosol hygroscopicity. Most heterogeneous atmospheric chemical processes in aerosols are acidity dependent (Yao et al., 2007). Strong acidity (H^+_{strong}), aerosol acidity (H^+_{air}), pH and water content of $PM_{2.1}$ at Huangshan and other compositions modeled by AIM-II are summarized in Table 4. It is noted that the model cannot predict the $[H^+_{air}]$ for fully neutralized aerosols, so these data were excluded from analysis. Finally, a total of 16 and 22 sets of daily data had valid output to evaluate the aerosol acidity of $PM_{2.1}$ at SM and LL, respectively. $[H^+]_{strong}$ ranged from 5.17 to 40.53 nmol/m^3 with the average of 19.08 nmol/m^3 at SM. The value was more variable at LL, ranging from 2.65 to 178.04 nmol/m^3 with the average of 36.10 nmol/m^3. Higher $[H^+]_{strong}$ at LL is in accordance with the higher concentrations of SO_4^{2-} and HSO_4^-. Compared with other mountainous sites in China, the aerosol acidity was highest at Mt. Tai (Zhou et al., 2012), with the value of $[H^+]_{air}$ 5–6 times higher than that of Huangshan. The acidity degree of Huangshan was the lowest for $[H^+]_{strong}$, $[H^+]_{air}$ and HSO_4^-, indicating that the atmospheric environment in Huangshan was relatively clean. An interesting finding was that the pH at Huangshan was lower than Mt. Heng (Gao et al., 2012), which may be associated with the low water content at Huangshan.

Water content in aerosol droplets plays a key role in the acidity of $PM_{2.1}$ (Pathak et al., 2003, 2009; Zhou et al., 2012). The interactions between water content and aerosol acidity are complicated. One is the release of free H^+ from HSO_4^- in the liquid phase of

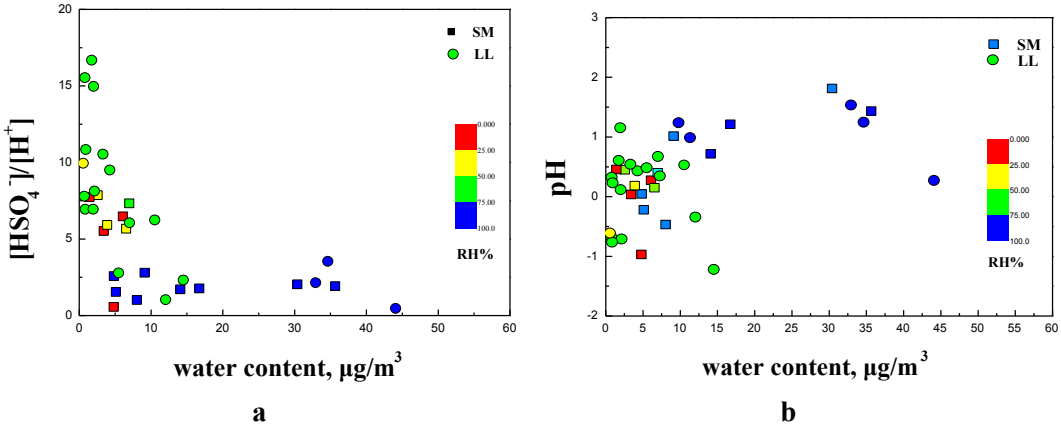

Fig. 8. (a) Molar ratio of $[HSO_4^-]$ to $[H^+]$ and (b) pH as a function of water content (colored by RH).

aerosol (Yao et al., 2007). To evaluate the impact of the HSO_4^- hydrolysis process on aerosol acidity, the ratio of $[HSO_4^-]/[H^+_{air}]$ against water content was examined (Fig. 8a). The estimated water content values were between 1.43 and 35.67 μg/m^3 at SM and between 0.56 and 44.07 μg/m^3 at LL. For water content less than 10 μg/m^3, the mole ratio of $[HSO_4^-]/[H^+_{air}]$ decreased with increasing water content, indicating that increasing aerosol water led to the dissociation of HSO_4^- to form free H^+. When RH increased to higher than 75%, the equivalent ratio of $[HSO_4^-]/[H^+_{air}]$ appeared to be less sensitive to the water content. This is because high RH causes more water into aerosols, favoring to uptake more SO_2, H_2SO_4 and HNO_3 and accelerate the oxidation of SO_2 in the aqueous phase to form new sulfate and nitrate. These will again uptake more water due to their hygroscopic characteristics to release more free H^+. On the other hand, high water content can also dilute proton concentrations in acidic aerosols, leading to the decrease of acidity in the aqueous phase (nmol/L). This is evidenced by increasing pH with increasing water content (Fig. 8b). pH hold a relatively low level with the average value of 0.12 at SM and 0.15 at LL when water content was very low at RH < 75%. When water content is higher than 10 μg/m^3, pH obviously increased with the average value of 1.29 at SM and 1.01 at LL.

4. Conclusion

In order to understand the vertical distributions of ions in aerosol particles along the mountain ridge, size-resolved measurement of aerosol particles and water-soluble inorganic ions (WSI) was conducted at two altitudes (SM: 1840 m a.s.l. and LL: 869 m a.s.l.) at Huangshan. The mass concentrations of $PM_{1.1}$, $PM_{2.1}$ and PM_{10} were 17.07, 21.28 and 39.25 μg/m^3, respectively, at SM and 24.79, 29.02 and 42.39 μg/m^3 at LL. Both the concentrations of aerosols and WSI decreased with increasing altitude. Ca^{2+} and NO_3^- were the major cation and anion in coarse particles while SO_4^{2-} and NH_4^+ were the major cation and anion in fine particles. SO_4^{2-} and NH_4^+ were mainly concentrated in fine mode. Nitrate exhibited bimodal size distribution at SM, but peaking in the coarse mode at LL. The particulate nitrate in coarse mode was formed by heterogeneous reaction on coarse particles containing Ca and Mg. The homogeneous gas-phase mechanism also acted as the main pathway of nitrate formation in ammonium-rich environment. Nitrate thermal volatilization under higher temperature conditions was responsible for the lower nitrate loadings in the fine mode at LL. Strong acidity (H^+_{strong}) and aerosol acidity (H^+_{air}) were higher at LL than SM. When compared with the aerosol acidity at Mt. Tai and Mt. Heng, it was weaker as the lower values of H^+_{strong}, H^+_{air} and HSO_4^- at Huangshan.

Acknowledgments

This study was funded by the National Natural Sciences Foundation of China (No. 41030962) and Research Foundation for the Introduction of Talent of Nanjing University of Information Science and Technology (2012X043). We gratefully thank Dr. Dantong Liu from the University of Manchester for polishing the language sincerely.

References

Andreae, M., Andreae, T., Annegarn, H., Beer, J., Cachier, H., Le Canut, P., Elbert, W., Maenhaut, W., Salma, I., Wienhold, F., 1998. Airborne studies of aerosol emissions from savanna fires in southern Africa: 2. Aerosol chemical composition. J. Geophys. Res. Atmos. 103, 32119–32128.

Andreae, M.O., Rosenfeld, D., 2008. Aerosol-cloud-precipitation interactions. Part 1. The nature and sources of cloud-active aerosols. Earth-Sci. Rev. 89, 13–41.

Cao, J., Shen, Z., Chow, J.C., Qi, G., Watson, J.G., 2009. Seasonal variations and sources of mass and chemical composition for PM_{10} aerosol in Hangzhou, China. Particuology 7, 161–168.

Chan, C., Xu, X., Li, Y., Wong, K., Ding, G., Chan, L., Cheng, X., 2005. Characteristics of vertical profiles and sources of $PM_{2.5}$, PM_{10} and carbonaceous species in Beijing. Atmos. Environ. 39, 5113–5124.

Chen, K., Yin, Y., Kong, S., Xiao, H., Wu, Y., Chen, J., Li, A., 2014. Size-resolved chemical composition of atmospheric particles during a straw burning period at Mt. Huang (the Yellow Mountain) of China. Atmos. Environ. 84, 380–389.

Cheng, S., Yang, L., Zhou, X., Xue, L., Gao, X., Zhou, Y., Wang, W., 2011. Size-fractionated water-soluble ions, situ pH and water content in aerosol on hazy days and the influences on visibility impairment in Jinan, China. Atmos. Environ. 45, 4631–4640.

Deng, C., Zhuang, G., Huang, K., Li, J., Zhang, R., Wang, Q., Liu, T., Sun, Y., Guo, Z., Fu, J., Wang, Z., 2011. Chemical characterization of aerosols at the summit of Mountain Tai in Central East China. Atmos. Chem. Phys. 11, 7319–7332.

Gao, X., Xue, L., Wang, X., Wang, T., Yuan, C., Gao, R., Zhou, Y., Nie, W., Zhang, Q., Wang, W., 2012. Aerosol ionic components at Mt. Heng in central southern China: abundances, size distribution, and impacts of long-range transport. Sci. Total. Environ. 433, 498–506.

Henning, S., Weingartner, E., Schwikowski, M., Gäggeler, H., Gehrig, R., Hinz, K.P., Trimborn, A., Spengler, B., Baltensperger, U., 2003. Seasonal variation of water-soluble ions of the aerosol at the high-alpine site Jungfraujoch (3580 m asl). J. Geophys. Res. Atmos. 108, 8–10. ACH 8-1-ACH.

Kong, S., Wen, B., Chen, K., Yin, Y., Li, L., Li, Q., Yuan, L., Li, X., Sun, X., 2014. Ion chemistry for atmospheric size-segregated aerosol and depositions at an offshore site of Yangtze River Delta region, China. Atmo. Res. 147-148, 205–226.

Lee, C., Chuang, M., Lin, N., Wang, J., Sheu, G., Chang, S., Wang, S., Huang, H., Chen, H., Liu, Y., Weng, G., Lai, H., Hsu, S.P., 2011. The enhancement of $PM_{2.5}$ mass and water-soluble ions of biosmoke transported from Southeast Asia over the Mountain Lulin site in Taiwan. Atmos. Environ. 45, 5784–5794.

Li, J., Wang, G., Zhou, B., Cheng, C., Cao, J., Shen, Z., An, Z., 2011a. Chemical composition and size distribution of wintertime aerosols in the atmosphere of Mt. Hua in central China. Atmos. Environ. 45, 1251–1258.

Li, W., Zhang, D., Shao, L., Zhou, S., Wang, W., 2011b. Individual particle analysis of aerosols collected under haze and non-haze conditions at a high-elevation mountain site in the North China plain. Atmos. Chem. Phys. 11, 11733–11744.

Li, W., Wang, Y., Collett Jr., J.L., Chen, J., Zhang, X., Wang, Z., Wang, W., 2013. Microscopic evaluation of trace metals in cloud droplets in an acid precipitation region. Environ. Sci. Technol. 47, 4172–4180.

Li, W., Chi, J., Shi, Z., Wang, X., Chen, B., Wang, Y., Li, T., Chen, J., Zhang, D., Wang, Z., 2014. Composition and hygroscopicity of aerosol particles at Mt. Lu in South China: Implications for acid precipitation. Atmos. Environ. 94, 626–636.

Liu, S., Hu, M., Slanina, S., He, L.Y., Niu, Y., Bruegemann, E., Gnauk, T., Herrmann, H., 2008. Size distribution and source analysis of ionic compositions of aerosols in polluted periods at Xinken in Pearl River Delta (PRD) of China. Atmos. Environ. 42, 6284–6295.

Ma, J., Xu, X., Zhao, C., Yan, P., 2012. A review of atmospheric chemistry research in China: photochemical smog, haze pollution, and gas-aerosol interactions. Adv. Atmos. Sci. 29, 1006–1026.

Manktelow, P., Carslaw, K., Mann, G., Spracklen, D., 2010. The impact of dust on sulfate aerosol, CN and CCN during an East Asian dust storm. Atmos. Chem. Phys. 10, 365–382.

Pathak, R.K., Yao, X., Lau, A.K., Chan, C.K., 2003. Acidity and concentrations of ionic species of $PM_{2.5}$ in Hong Kong. Atmos. Environ. 37, 1113–1124.

Pathak, R.K., Wu, W., Wang, T., 2009. Summertime $PM_{2.5}$ ionic species in four major cities of China: nitrate formation in an ammonia-deficient atmosphere. Atmos. Chem. Phys. 9, 1711–1722.

Rosenfeld, D., Dai, J., Yu, X., Yao, Z., Xu, X., Yang, X., Du, C., 2007. Inverse relations between amounts of air pollution and orographic precipitation. Science 315, 1396–1398.

Shen, Z., Cao, J., Arimoto, R., Han, Z., Zhang, R., Han, Y., Liu, S., Okuda, T., Nakao, S., Tanaka, S., 2009. Ionic composition of TSP and $PM_{2.5}$ during dust storms and air pollution episodes at Xi'an, China. Atmos. Environ. 43, 2911–2918.

Takeuchi, M., Okochi, H., Igawa, M., 2004. Characteristics of water-soluble components of atmospheric aerosols in Yokohama and Mt. Oyama, Japan from 1990 to 2001. Atmos. Environ. 38, 4701–4708.

Tian, Y., Shi, G., Han, S., Zhang, Y., Feng, Y., Liu, G., Gao, L., Wu, J., Zhu, T., 2013. Vertical characteristics of levels and potential sources of water-soluble ions in PM_{10} in a Chinese megacity. Sci. Total. Environ. 447, 1–9.

Vedal, S., Hannigan, M., Dutton, S., Miller, S., Milford, J., Rabinovitch, N., Kim, S.Y., Sheppard, L., 2009. The Denver Aerosol Sources and Health (DASH) study: overview and early findings. Atmos. Environ. 43, 1666–1673.

Wang, G., Kawamura, K., Umemoto, N., Xie, M., Hu, S., Wang, Z., 2009. Water-soluble organic compounds in $PM_{2.5}$ and size-segregated aerosols over Mount Tai in North China Plain. J. Geophys. Res. Atmos. 114, D19208.

Wang, G., Li, J., Cheng, C., Hu, S., Xie, M., Gao, S., Zhou, B., Dai, W., Cao, J., An, Z., 2011. Observation of atmospheric aerosols at Mt. Hua and Mt. Tai in central and east China during spring 2009 – Part 1: EC, OC and inorganic ions. Atmos. Chem. Phys. 11, 4221–4235.

Wang, H., Zhu, B., Shen, L., Kang, H., 2012a. Size distributions of aerosol and water-soluble ions in Nanjing during a crop residual burning event. J. Environ. Sci. 24, 1457–1465.

Wang, Z., Wang, T., Guo, J., Gao, R., Xue, L., Zhang, J., Zhou, Y., Zhou, X., Zhang, Q., Wang, W., 2012b. Formation of secondary organic carbon and cloud impact on carbonaceous aerosols at MountTai, North China. Atmos. Environ. 46, 516–527.

Wang, Y., Zhuang, G., Tang, A., Yuan, H., Sun, Y., Chen, S., Zheng, A., 2005. The ion chemistry and the source of $PM_{2.5}$ aerosol in Beijing. Atmos. Environ. 39, 3771–3784.
Yao, X., Yan, L., Fang, M., Chan, C.K., 2006. Comparison of thermodynamic predictions for in situ pH in $PM_{2.5}$. Atmos. Environ. 40, 2835–2844.
Yao, X., Yan, L.T., Fang, M., Chan, C.K., 2007. Size dependence of in situ pH in submicron atmospheric particles in Hong Kong. Atmos. Environ. 41, 382–393.
Zhang, L., Vet, R., Wiebe, A., Mihele, C., Sukloff, B., Chan, E., Moran, M., Iqbal, S., 2008. Characterization of the size-segregated water-soluble inorganic ions at eight Canadian rural sites. Atmos. Chem. Phys. 8, 7133–7151.
Zhang, T., Cao, J., Tie, X., Shen, Z., Liu, S., Ding, H., Han, Y., Wang, G., Ho, K., Qiang, J., 2011. Water-soluble ions in atmospheric aerosols measured in Xi'an, China: seasonal variations and sources. Atmos. Res. 102, 110–119.
Zhao, J., Zhang, F., Xu, Y., Chen, J., 2011. Characterization of water-soluble inorganic ions in size-segregated aerosols in coastal city, Xiamen. Atmos. Res. 99, 546–562.
Zhao, Y., Gao, Y., 2008. Mass size distributions of water-soluble inorganic and organic ions in size-segregated aerosols over metropolitan Newark in the US east coast. Atmos. Environ. 42, 4063–4078.
Zhou, Y., Wang, T., Gao, X., Xue, L., Wang, X., Wang, Z., Gao, J., Zhang, Q., Wang, W., 2009. Continuous observations of water-soluble ions in $PM_{2.5}$ at Mount Tai (1534 m asl) in central-eastern China. J. Atmos. Chem. 64, 107–127.
Zhou, Y., Xue, L., Wang, T., Gao, X., Wang, Z., Wang, X., Zhang, J., Zhang, Q., Wang, W., 2012. Characterization of aerosol acidity at a high mountain site in central eastern China. Atmos. Environ. 51, 11–20.